Turbulent Structure in Steep Open-Channel Flows

by

Akihiro TOMINAGA and Iehisa NEZU†

(Received March 29, 1991)

Abstract

Velocity measurement with a fiber-optic laser-Doppler anemometer were conducted in steep open-channel flows over smooth and incompletely rough beds. The channel slopes were changed between 1/500 and 1/25 by steps, and as a result, the Froude number changed from 0.5 to 3. The law of the wall and the distributions of turbulence intensity were examined in more detail. The von Kármán constant κ in the log law was verified to be unversally equal to 0.41. On the other hand, the integral constant A in the log law coincided with the usual value of 5.29 in subcritical flows, whereas it decreased with an increase of the bed slope in supercritical flows. This decrease of A was explained by a decrease of the damping factor B in the van Driest's mixing-length formula. The decrease of B was well correlated with an increase of the friction velocity and the roughness. The streamwise turbulence intensity became smaller in the near-wall region than the semi-empirical universal formula, as the friction velocity became larger.

1. Introduction

It is necessary to clarify the velocity profile and the resistance law in steep open-channel flows in order to solve the problems of soil erosion and sediment transport on steep slopes. However, it has been difficult to accurately measure the flow structures in such steep open-channel flows, because of very high velocity fluctuations and relatively small flow depth. Ishihara et al. (1951) and Iwagaki (1953) have measured the velocity profiles in smooth thin-sheet flows, using a very small Pitot tube with 0.92 mm diameter. They found that the integral constant A of the log-law distribution became smaller with an increase of the Froude number, and hence they introduced the Froude number into the resistance law of the thin-sheet flows.

Some researchers have studied the resistance law in steep open-channel flows, but most of them have treated the flows over rough beds in order to establish the resistance law of a mountain river (e. g. Ashida et al., 1973 and Kanda et al., 1979, 1981). Nezu (1977) investigated the effect of Froude number on turbulent structures

Department of Civil Engineering, Nagoya Institute of Technology, Nagoya 466, Japan.
† Division of Global Environment Engineering, Kyoto University, Kyoto 606, Japan..

in open-channel flows, and he concluded that the properties of turbulence dimensionlessed by the outer variables, i.e. the friction velocity U_* and the flow depth h, were not affected by the Froude number except for the case of the near-critical flows. Recently, Nezu & Rodi (1986) have accurately measured the velocity distributios in smooth open-channel flows by making use of a Laser Doppler Anemometer (LDA). They established that the von Kármán constant κ in the log-law distributions was a universal constant, i.e. $\kappa = 0.412$, and the integral constant A was nearly equal to 5.29, irrespective of the Reynolds and Froude numbers. However, the range of the Froude number in their experiments was limited below 1.24. Many investigations have been conducted into the velocity profiles in turbulent flows over smooth and rough boundaries, analytically (e. g. Coleman et al., 1981, Sill, 1982, Wills, 1985 and Vedura, 1985) and also experimentally using Pitot tube and hot-film anemometer (Cardoso et al., 1989) and Laser Doppler anemometer (Kirkgöz, 1989). However, more detailed information about the Kármán constant κ and the integral constant A is not yet available in steep open-channel flows, in which the supercritical flows are fully developed.

Considering the above, in this study, the velocity measurements were accurately conducted in steep open-channel flows over smooth and rough beds by making use of a fiber-optic Laser-Doppler anemometer. From these experiments, the reduction of the integral constant A in the log-law distribution was found in the case of supercritical flows. This important phenomenon could be explained on the basis of the mixing-length theory. The characteristics of turbulence intensity were also investigated in steep open-channel flows.

2. Experimental Apparatus and Procedure

The experiments were conducted in two different flumes, **A** and **B**. Flume **A** was 4m long and 0.2m wide, and was made of acrylic-resin plate. Flume **B** was 12.5m long and 0.4m wide. The bed wall was composed of vinyl-chloride plate and the side walls were composed of glass. Flume **A** was used for experiments with thin-sheet open-channel flows. In this case, the bed slope was changed from 1/500 to 1/25 in 5 steps, and flow depth h was changed from 3mm to 15mm in 4 or 5 steps for each bed slope. In the case of rough bed, the sandpaper (the mean diameter of sand was approximately 0.1mm) was pasted over the smooth bed of flume **A**. The hydraulic conditions for rough bed were set up in the same manner as for the smooth bed. On the other hand, in flume **B**, the bed slope was changed from 1/500 to 1/54 in 4 steps, and flow depth h was changed from 5mm to 40mm in 4 steps for each bed slope. Velocity was measured at the test sections located 3m (for flume **A**)

and 7.5m (for flume **B**) downstream from the entrance of each channel. In these sections, the flow was fully developed and approximately uniform. This was confirmed by the fact that the velocity profile obtained 0.5m upstream from the test section coincided with that at the test section. In all cases, no significantly large water waves such as a rolling wave were observed.

All of the experimental conditions are shown in Table 1, in which U_m is the mean velocity obtained from the integrated velocity profile and U_* is the friction velocity. Since the flow was fully-developed and uniform in all experiments, the friction velocity U_* was evaluated as $U_* = \sqrt{ghI}$ (g = gravitational acceleration and I = bed slope), which was recognized as the value at the center of the channel. Since the measurement of the bed slope becomes more accurate with an increase of the bed slope, the accuracy of the eveluation of U_* is fairly high in these steep open channel flows. The Froude number $\mathrm{Fr} \equiv U_m/\sqrt{gh}$ was widely changed from 0.5 to 3, i.e. from subcritical to supercritical flows. The Reynolds number $\mathrm{Re} = U_m h/\nu$ (ν = kinetic visocity) changed from 300 to 6×10^4, i.e. from laminar to turbulent flows. Nezu et al. (1985, 1989) and Tominaga et al. (1989) found that signifiant secondary currents appeared in the whole section of the narrow open channels with aspect ratio $b/h \leqq 5$ (b = channel width), whereas no secondary currents appeared in the central zone, i.e., $|z/h| < (5 - b/h)/2$ in the case of wide open channels. Since the aspect ratio b/h was larger than 10 as indicated in Table 1, it was oncluded that all the flows of the present experiments were two-dimensional, i.e. no secondary currents, in the central zone of the channel.

Accurate measurements of the velocity components were carried out by making use of a two-color four-beam fiber-optic Laser Doppler anemometer (FLDA). A 2W high-power Argon-ion laser was used as a light source. The same FLDA measurement system was used in the study of compound open-channel flows and the more detailed information is given in our paper (Tominaga & Nezu, 1990). The streamwise velocity component u was measured by a two beam method. This FLDA system enabled us to measure the velocity with a high accuracy in high-speed thin-sheet flows, becuase no probe was introduced in the water and the measuring volume was very small, i.e. $\Delta y = 0.15$mm. The measuring point closest to the bed was set up at 0.1mm distant from the bed, and the minimum distance of the traverse was 0.1mm in the region near the bed. The origin of the vertical coordinate of the measuring point was determined by the visual adjustment of the FLDA focus point, and it was then corrected to fit the velocity profile to the theoretical one in the viscous sublayer. The maximum value of the correction length was only $\pm$ 0.2mm. The output signals from the frequency trackers were digitized using an A-D converter with sampling frequencies of 100 or 200 Hz and a sampling time of

Table 1. Experimental Conditions

(a) smooth (flume A)

CASE	Bed Slope I	Flow Depth h (mm)	Aspect Ratio b/h	Mean Velocity U_m (cm/s)	Friction Velocity U_* (cm/s)	Froude Number Fr	Reynolds Number Re ($\times 10^3$)
A-01	1/25	9.5	21	92.9	6.11	3.05	7.4
A-02	〃	8.0	25	84.7	5.60	3.01	5.6
A-03	〃	5.5	36	66.5	4.65	2.87	3.1
A-04	〃	3.5	57	47.7	3.70	2.56	1.4
A-05	1/50	11.1	18	71.7	4.66	2.13	6.6
A-06	〃	9.0	22	61.7	4.20	2.06	4.7
A-07	〃	6.0	33	47.5	3.44	1.94	2.5
A-08	〃	3.7	54	32.9	2.69	1.80	1.1
A-09	1/100	13.9	14	60.2	3.69	1.55	6.7
A-10	〃	11.2	18	52.1	3.35	1.53	4.9
A-11	〃	8.1	25	42.4	2.84	1.45	2.9
A-12	〃	5.9	34	34.4	2.42	1.36	1.7
A-13	〃	3.8	53	26.6	1.93	1.27	0.82
A-14	1/250	16.3	12	39.8	2.52	0.93	5.1
A-16	〃	11.2	18	30.9	2.16	0.86	2.7
A-17	〃	8.9	23	27.6	1.97	0.88	2.0
A-18	〃	5.3	38	21.5	1.42	0.94	0.98
A-19	〃	3.3	61	11.5	1.19	0.64	0.33
A-20	1/500	15.3	13	28.1	1.71	0.67	3.4
A-21	〃	10.9	18	21.3	1.54	0.62	1.9
A-22	〃	8.1	25	16.6	1.22	0.57	1.1
A-23	〃	5.3	38	11.6	0.94	0.51	0.53

(b) rough (flume A)

CASE	Bed Slope I	Flow Depth h (mm)	Aspect Ratio b/h	Mean Velocity U_m (cm/s)	Friction Velocity U_* (cm/s)	Froude Number Fr	Reynolds Number Re ($\times 10^3$)
B-01	1/25	3.3	61	42.3	3.59	1.75	1.0
B-02	〃	5.8	35	49.6	4.75	1.62	2.2
B-03	〃	8.0	25	71.6	5.60	2.22	4.9
B-04	〃	10.2	20	84.9	6.33	2.36	7.5
B-05	〃	15.6	13	108.4	7.81	2.54	15.0
B-06	1/50	3.3	61	30.0	2.54	1.39	0.80
B-07	〃	5.6	36	42.4	3.30	1.55	2.0
B-08	〃	8.2	24	57.4	4.01	1.74	4.0
B-09	〃	10.2	20	65.6	4.47	1.81	5.8
B-10	〃	15.1	13	81.3	5.44	1.98	11.0
B-11	1/100	3.2	63	25.4	1.78	1.22	0.67
B-12	〃	5.0	40	28.5	2.21	1.18	1.2
B-13	〃	8.1	25	41.7	2.81	1.36	3.0
B-14	〃	10.3	19	47.9	3.18	1.37	4.4
B-15	〃	15.1	13	60.5	3.84	1.45	8.1
B-16	1/250	3.2	63	12.5	1.12	0.60	0.34
B-17	〃	5.2	39	20.9	1.42	0.79	0.91
B-18	〃	8.3	24	26.7	1.80	0.85	2.0
B-19	〃	10.2	20	30.2	2.00	0.87	2.8
B-20	〃	15.0	13	39.7	2.43	0.92	5.3
B-21	1/500	3.5	57	6.7	0.82	0.32	0.19
B-22	〃	5.2	39	14.6	1.01	0.59	0.68
B-23	〃	8.4	24	18.3	1.28	0.60	1.4
B-24	〃	10.4	20	22.2	1.42	0.63	2.0
B-25	〃	15.1	13	28.9	1.72	0.68	3.9

(c) smooth (flume B)

CASE	Bed Slope I	Flow Depth h (mm)	Aspect Ratio b/h	Mean Velocity U_m (cm/s)	Friction Velocity U_* (cm/s)	Froude Number Fr	Reynolds Number Re ($\times 10^3$)
C-01	1/54	6.3	64	48.2	3.38	2.08	3.2
C-02	〃	11.3	35	76.4	4.53	2.32	9.1
C-03	〃	19.2	21	110.5	5.90	2.46	22.0
C-04	〃	28.8	14	138.9	7.23	2.49	41.0
C-05	〃	38.8	10	152.5	8.39	2.45	62.0
C-06	1/100	6.3	64	37.1	2.47	1.79	2.9
C-07	〃	12.1	33	59.2	3.44	1.82	7.9
C-08	〃	25.8	15	98.6	5.03	1.95	28.0
C-09	〃	35.1	11	115.8	5.86	1.94	44.0
C-10	1/250	6.3	64	24.7	1.57	1.40	2.1
C-11	〃	11.4	35	35.4	2.12	1.10	4.2
C-12	〃	22.5	18	54.9	2.97	1.22	13.0
C-13	〃	40.3	10	77.5	3.97	1.25	33.0
C-14	1/500	5.8	69	15.6	1.07	1.18	1.7
C-15	〃	10.0	40	20.3	1.40	0.84	2.8
C-16	〃	20.8	19	34.0	2.02	0.81	8.3
C-17	〃	30.5	13	44.8	2.45	0.83	15.0

41 seconds.

3. Mean Velocity Distributions

Fig. 1 shows an example of the mean velocity distribution in the case of the very low Reynolds numbers $Re = 530$ and $Re = 1100$. The solid line in this figure

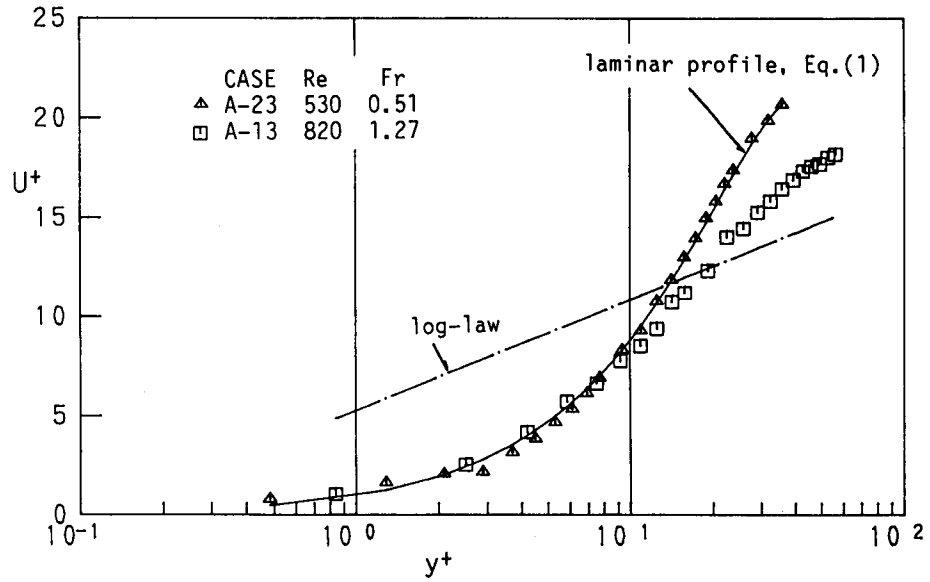

Fig. 1 Examples of Laminar and Transitional Velocity Profile

describes the theoretical profile of the laminar flow, as follows:

$$U^+ = y^+(1 - y/2h) \tag{1}$$

in which $U^+ = U/U_*$ and $y^+ = U_* y/\nu$. Since the experimental values coincide well with the theoretical curve of Eq. (1), it is concluded that the open-channel flow at $Re = 530$ is surely laminar. Such good agreement between theoretical and experimental values also indicates that the present FLDA measurements of velocity are very accurate. The velocity profile at $Re = 1100$ deviates from the laminar profile of Eq. (1) near the free surface. This suggests a transition from laminar to turbulent flow.

Fig. 2 shows several examples of the mean velocity profiles in fully-turbulent range at moderate Reynolds numbers. Figs. 2 (a), (b) and (c) show the variation of the velocity profiles as a function of bed slope I in the case of (a) a smooth bed, (b) a rough bed in flume **A** and (c) a smooth bed in flume **B**, respectively. The well-known formula of "the law of the wall" is as follows:

$$U^+ = y^+ \qquad (y^+ < 5) \tag{2}$$

$$U^+ = \frac{1}{\kappa}\ln(y^+) + A \quad (y^+ > 30) \tag{3}$$

in which κ is the von Kármán constant and A is the integral constant. Although $\kappa = 0.4$ and $A = 5.5$ were given for pipe flows by Nikuradse (e.g. see Schlichting, 1979), the values of $\kappa = 0.412$ and $A = 5.29$ were recently obtained by Nezu & Rodi (1986) for open channel flows. The calculated curves of Eqs. (2) and (3) are shown in Fig. 2.

Since the Froude number Fr is given by

$$Fr = \frac{U_m}{\sqrt{gh}} = \left(\frac{U_m}{U_*}\right)\sqrt{I} \tag{4}$$

and the value of (U_m/U_*) does not so largely change in the identical roughness condition, the Froude number represents the effect of bed slope I.

The present experimental data indicate that the Kármán constant κ does not change even in steep open-channel flows such as $I = 1/25$ and $1/100$, but that the integral constant A decreases with an increase of the bed slope I. This feature is consistent with the previous experimental data at high Froude numbers obtained by Ishihara et al. (1951). It should be noted that A decreases with an increase of the Reynolds number Re when the Froude number is kept as a high constant, i.e. a supercritical flow, as clearly seen in Fig. 2 (c); compare C-05 with C-03 and C-04.

Fig. 3 shows the variations in the experimental value of the Kármán constant κ

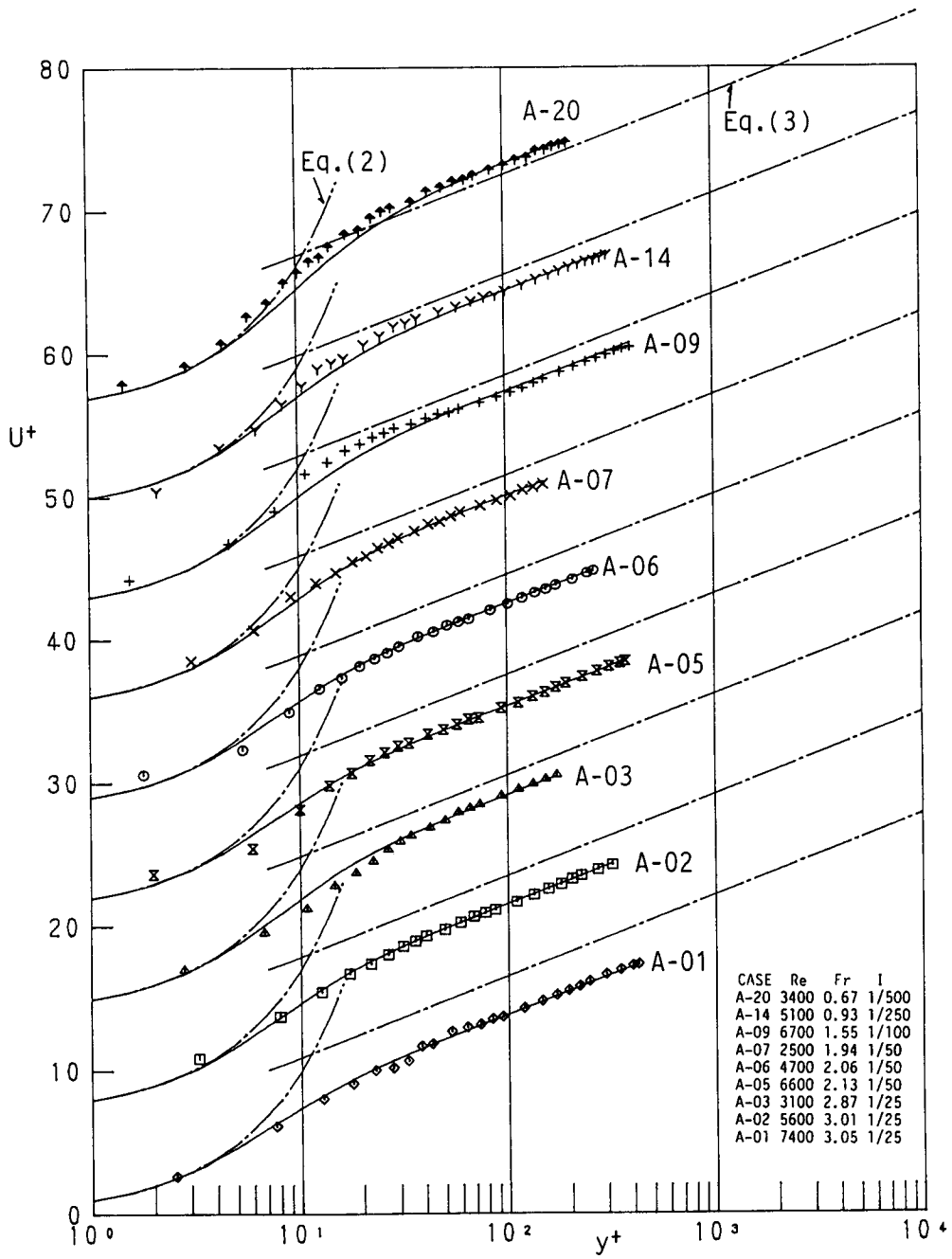

(a) Case A (smooth, flume A)

Fig. 2 Mean Velocity Profiles in Turbulent Flow

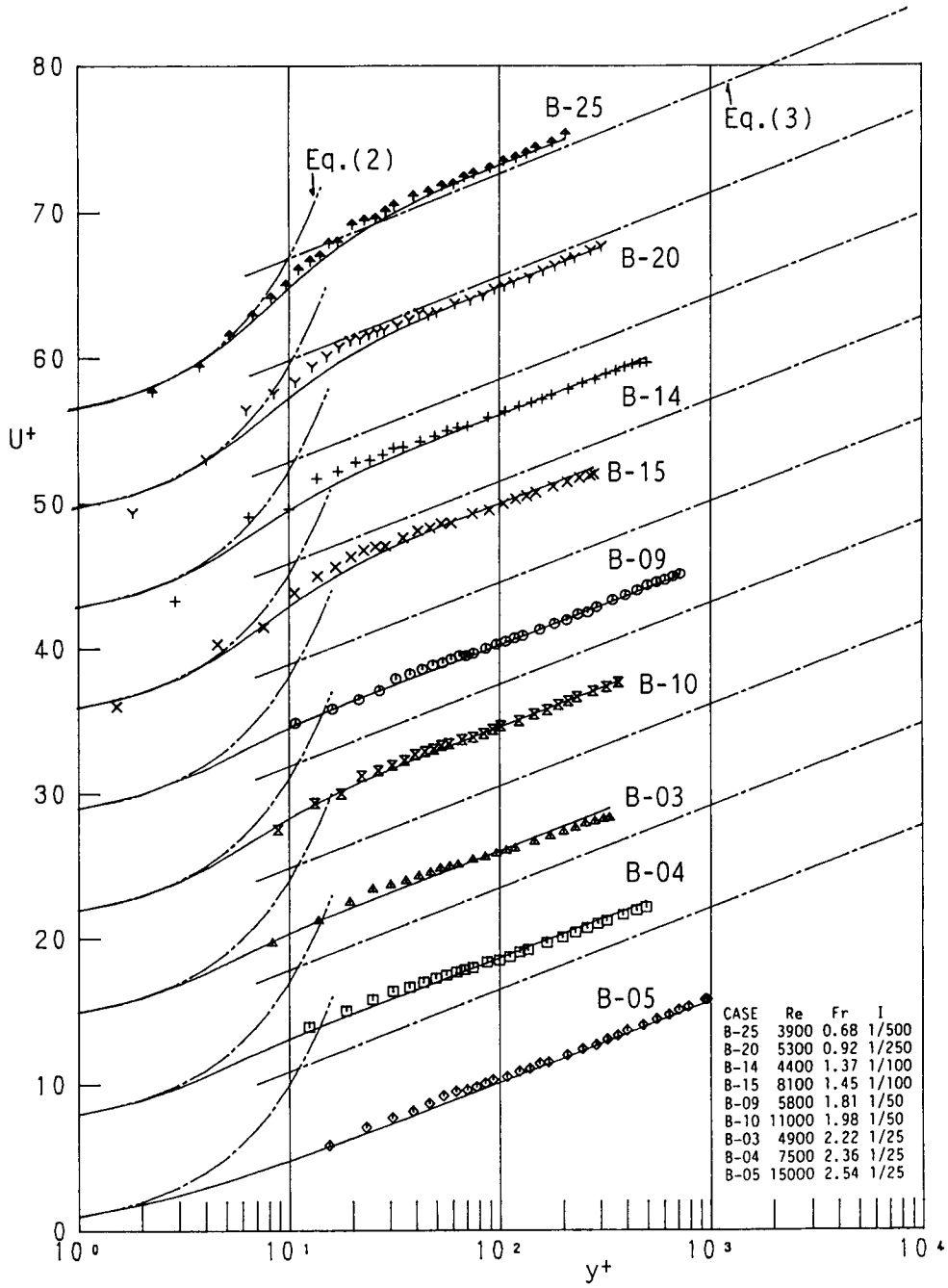

(b) Case B (rough, flume A)

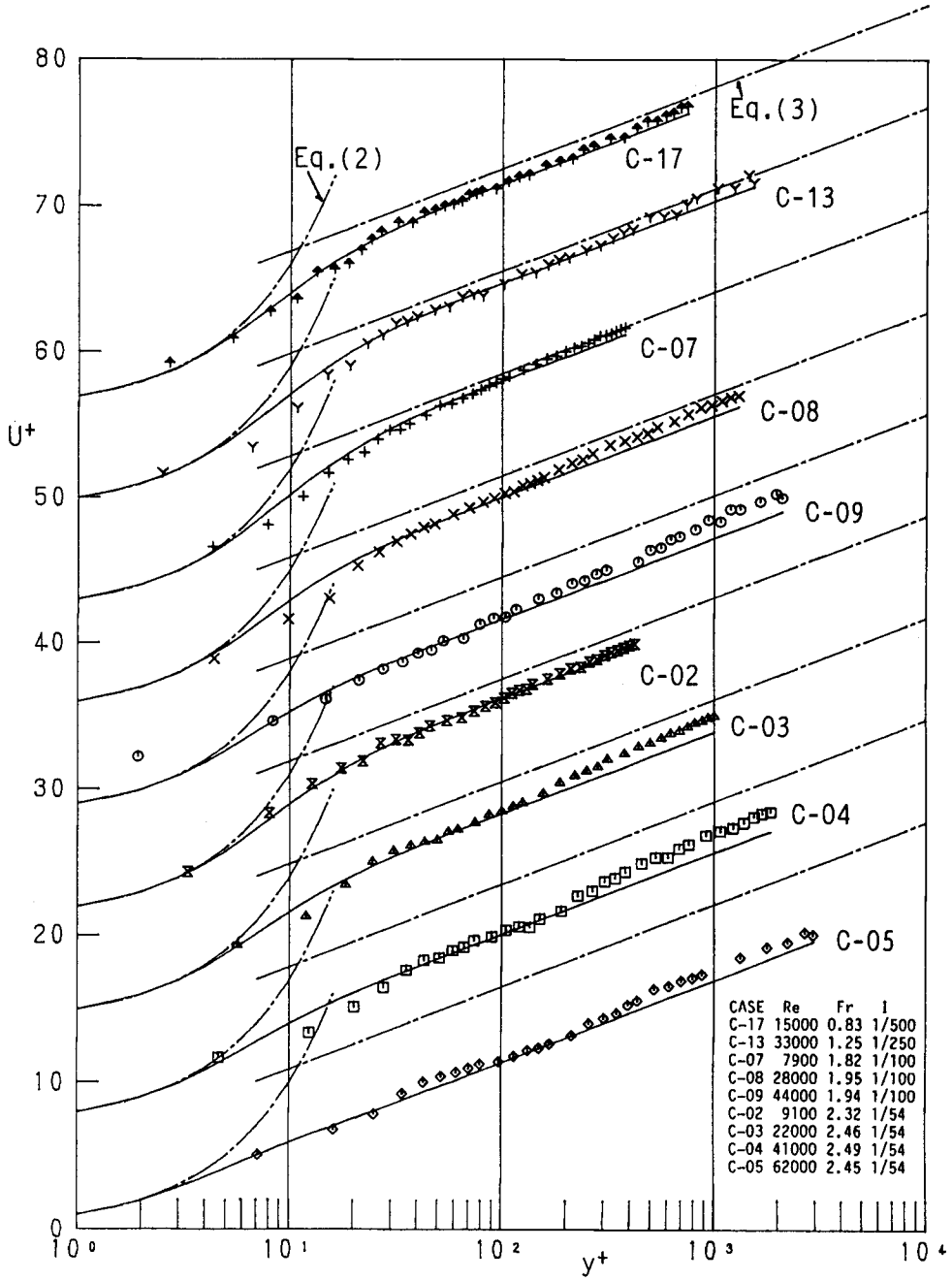

(c) Case C (smooth, flume B)

against the Froude number Fr in all experimental cases. The value of κ was evaluated from the linear regression of the experimental values of velocity in the semi-log diagram. The values of κ overlap well with the universal constant of 0.41

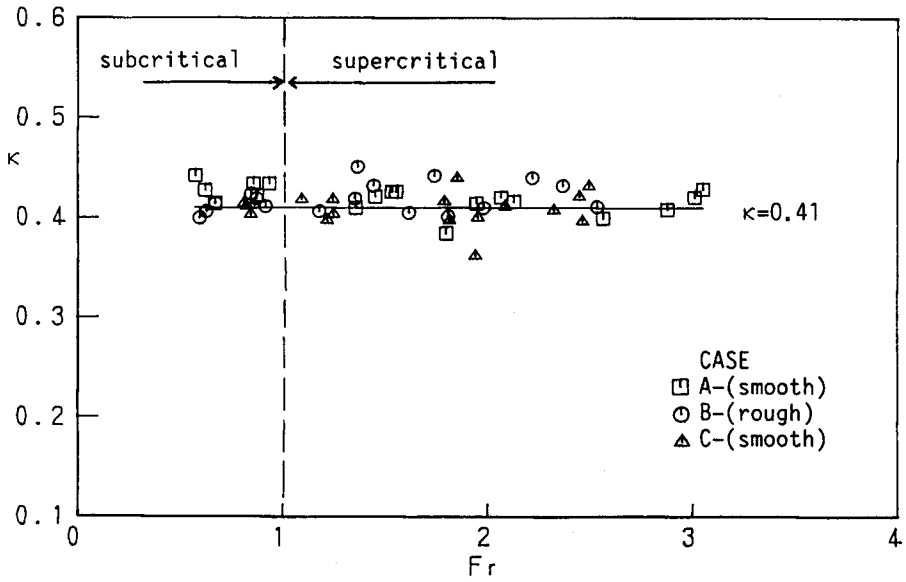

Fig. 3 Kármán Constant κ against Froude Numer

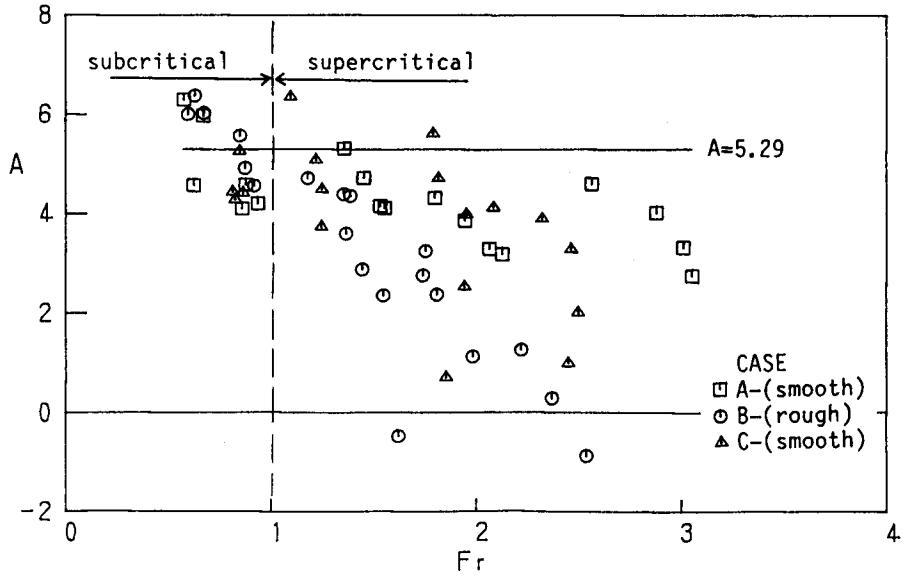

Fig. 4 Integral Constant A against Froude Number

without any systematic scatter, against the Froude number. Therefore, it is concluded that κ is a universal constant, i.e. $\kappa = 0.41$, even in the steep open-channel flows.

On the other hand, Fig. 4 shows the variations of the integral constant A, which was evaluated from the linear regresion of the log-law with the fixed value of $\kappa = 0.41$. The experimental values of A coincide fairly well with $A = 5.29$ obtained by Nezu & Rodi (1986) in the subcritical flows, whereas they decrease from $A = 5.29$ with an increase of the Froude number in the supercritical flows. The same features have been pointed out by Iwagaki (1953) who measured the velocity distributions in steep sheet-flows with a small Pitot tube.

Although there are large scatters among the experimental values of A, it should be noted that the decrease of A is larger over the rough bed than over the smooth bed at the same Froude numbers. Such a decrease of A implies that the thickness δ of the viscous sublayer becomes smaller, as clearly seen in Fig. 2 (b). This fact suggests strongly that the viscous effect may become weaker in supercritical steep open-channel flows and enventually its effect may disappear over rough beds in such flows. These noticeable features are explained on the basis of the mixing-length theory in the following section.

4. Law of the Wall and Mixing-Length Theory

The streawise equation of motion in fully-developed two-dimensional flow is reduced to the following equation of the total shear stress τ:

$$\frac{\tau}{\rho} = -\overline{uv} + \nu\frac{dU}{dy} = U_*^2(1-\xi) \tag{5}$$

in which $\xi = y/h$ and ρ is the density of water. $\rho\nu(dU/dy)$ is the viscous stress, while $-\rho\overline{uv}$ is the Reynolds stress. According to the Prandtl's mixing-legth model, the Reynolds stress $-\rho\overline{uv}$ is expressed by

$$-\rho\overline{uv} = \rho l^2\left|\frac{dU}{dy}\right|\frac{dU}{dy} \tag{6}$$

in which l is the mixing length. By substituting Eq. (6) into Eq. (5), the following equation is obtained:

$$\frac{dU^+}{d\xi} = \frac{2R_*(1-\xi)}{1+\sqrt{1+4l^{+2}(1-\xi)}} \tag{7}$$

in which $R_* = U_*h/\nu$ and $l^+ = U_*l/\nu$. By integrating Eq. (7) on an appropriate

assumption about the mixing-length l, the velocity profile is calculated for the whole the region, i.e. from the viscous sublayer, through the buffer layer, to the fully turbulent layer. As to the mixing length, Prandtl gave a linear distribution:

$$l = \kappa y \tag{8}$$

On the other hand, Iwagaki(1953) considered that the decrease of the integral constant A in supercitical flows would be caused by the change of the mixing length due to the instability of the free surface, and he assumed then the following relations:

$$l = \kappa'(y - \delta_L) \qquad \text{for } \delta_L^+ < y^+ < 100$$

$$l = \kappa(y - \delta_L) + l_w \qquad \text{for } y^+ > 100$$

in which $\kappa' = \kappa + l_w/(100 - \delta_L^+)$. δ_L is the thickness of the viscous sublayer, i.e. $\delta_L^+ \simeq 10$. The superscipt "$^+$" means mormalization by the inner variables, i.e. U_* and ν/U_*. l_* is the amount of an increase of the mixing length due to the free-surface instability. However, the reduction of the viscous-sublayer thickness in supercritical flows was not considered in Iwagaki's model.

On the other hand, van Driest (1956) introduced a damping function into the linear distribution of the mixing-length, Eq. (8), to describe the viscous effect near the wall, as follows:

$$l = \kappa y \cdot \Gamma \tag{9}$$

$$\Gamma = 1 - exp(-y^+/B) \tag{10}$$

in which Γ is the damping function and B is the damping coefficient. It is well known that this van Driest's model with $B = 26$ very well reproduces the experimental values of the velocity profile in subcritical flows (see e.g. Nezu & Rodi, 1986). For the description of the overall profile, it is necessary to consider the effect of the linear decrease of the shear strees, i.e. Eq. (5). Then,

$$l = \kappa y \Gamma \sqrt{(1 - \xi)} \tag{11}$$

is finally obtained as the functin of the mixing length. Furthermore, Nezu & Rodi (1986) found that the wake effect appeared in the outer region of $\xi > 0.2$ at a high Reynolds number, i.e. $Re > 10^5/4 = 2.5 \times 10^4$.

In the case of thin sheet flows, i.e. cases **A** and **B**, no wake effect appeared, as seen in Figs 2 (a) and (b), because the Reynolds number Re was relatively low, i.e. $Re < 1.5 \times 10^4$, as shown in Table 1. In such cases, Eq. (10) is satisfied in all the regions from the wall to the free surface. In the case of C, an apparent wake effect was observed at $Re > 2 \times 10^4$, as seen in Fig. 2 (c). In this study, the wake effect is,

however, not considered, because the flow behaviour in the outer region does not play a significant role for the decrease of constant A in the log law.

The damping function Γ describes the rate of the penetration of turbulence into the viscous sublayer. That is, $\Gamma = 1$ means a fully-turbulent flow, whereas $\Gamma = 0$ means a non-turbulent flow. The damping coefficient B is correlated with the thickness of the buffer layer. Fig. 5 shows the variation of the mixing length against y^+ as a functin of B, which were calculated from Eqs. (10) and (11). The mixing length near the wall increases with a decrease of B. Fig. 6 shows the variation of the velocity profile calculated by integrating Eq. (7), as a parameter of B. Of particular significance is that the Kármán constant κ is certainly universal, i.e. $\kappa = 0.41$, irrespective of B, whereas the integral constant A becomes smaller with an decrease of B. The values of B were determined so that the calculated velocity profile of Eq. (7) might coincide with the experimental values. These calculated profiles have been indicated already by solid lines in Fig. 2, and they agree well with the experimental values. The relation between the observed values of A and B is shown in Fig. 7. The following approximated formula is empirically obtained from this diagram of Fig. 7.

$$A = -0.002B^2 + 0.286B - 0.952 \qquad \text{for } \kappa = 0.41 \tag{12}$$

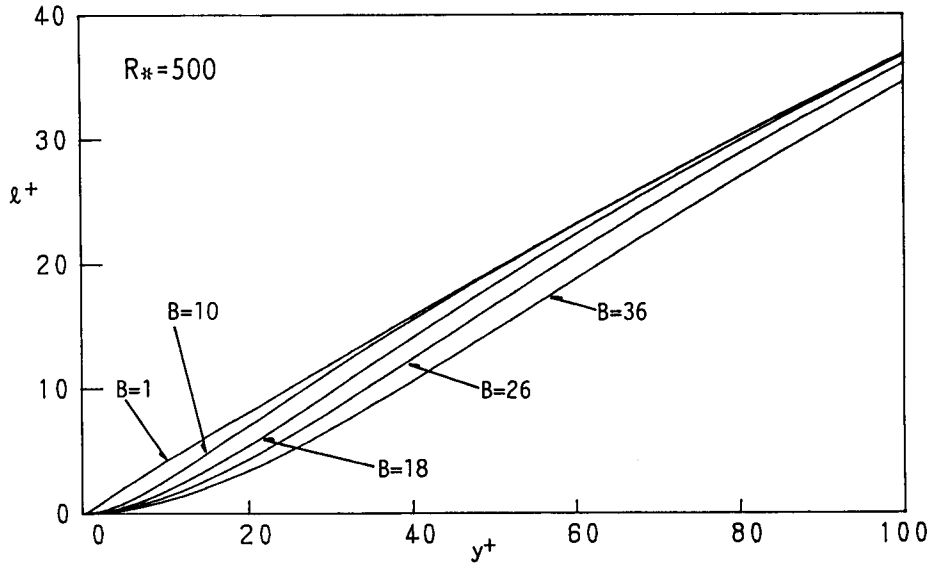

Fig. 5 Variation of Mixing Length Distribution as a functin of B (van Driest's Model)

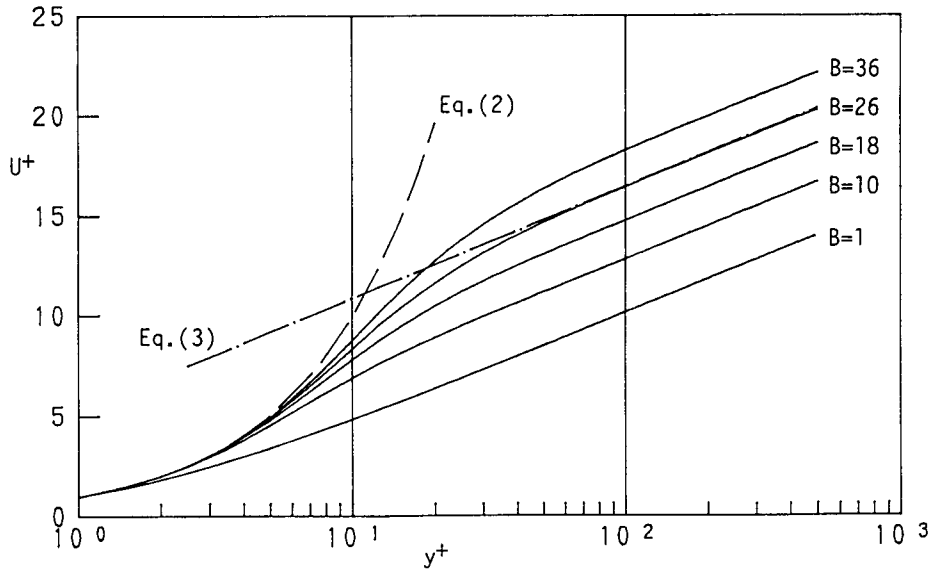

Fig. 6 Calculated Velocity Profiles as a function of B (van Driest's Model)

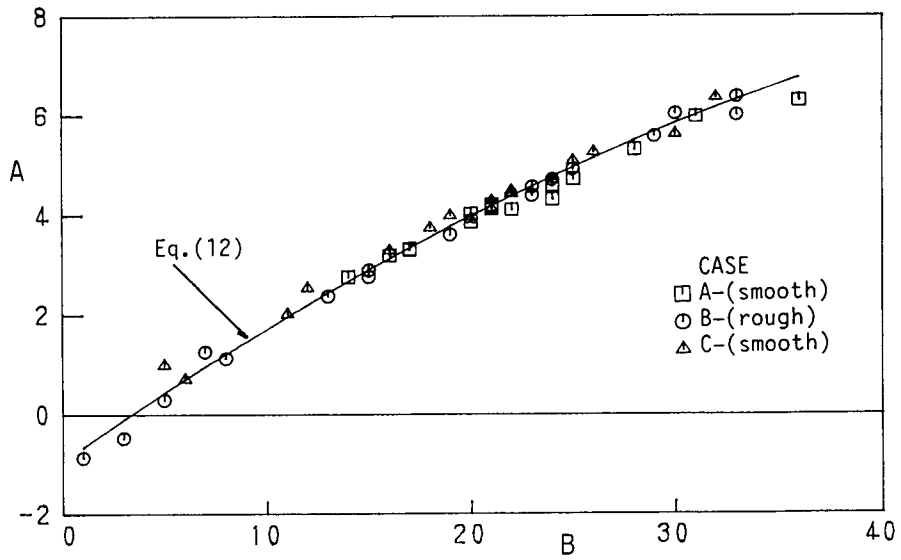

Fig. 7 Relation between Integral Coefficient, A, and Damping Coefficient, B

The above-mentioned van Driest's model becomes invalid for the completely rough bed in which the viscous sublayer disappears throughout. In this rough case, a concept of "the theoretical origin" should be introduced in which the mixing length is not zero any longer at the origin of the bed (see e.g. Coleman & Alonso, 1981, Sill, 1982 and Wills, 1985). In order to incorporate the effect of boundary roughness, Cebeci & Chang (1978) modified Eqs. (9) and (10) by substituting $y^+ + \Delta y^+$ for y^+, that is;

$$l^+ = \kappa(y^+ + \Delta y^+)\cdot\Gamma \tag{13}$$

$$\Gamma = 1 - \exp(-(y^+ + \Delta y^+)/B) \tag{14}$$

They introduced the shift of distance from the bed, Δy^+, which is empirically given by

$$\Delta y^+ = 0.9[(k_s^+)^{1/2} - k_s^+ \exp(-k_s^+/6)] \tag{15}$$

in which $k_s^+ = k_s U_*/\nu$, and k_s is the equivalent sand roughness. This expression is valid for $k_s^+ < 2000$ and Eqs. (13) and (14) are reduced to Eqs. (9) and (10) as k_s^+ approaches zero. The velocity distributions calculated from Eqs. (13) and (14) are shown in Fig. 8 for the different values of k_s^+. Cobeci & Chang's model can represent the relevant velocity profiles which indicate the decrease of the constant A

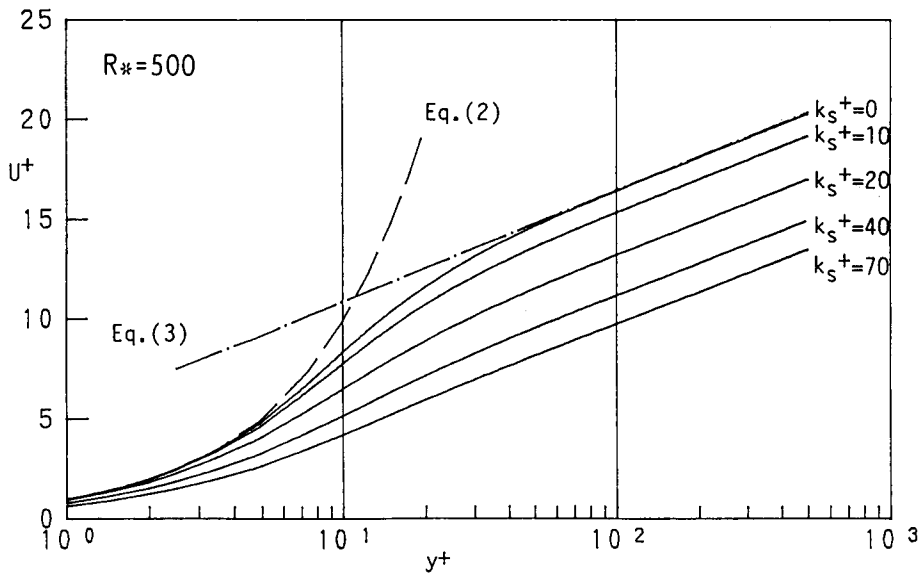

Fig. 8 Calculated Velocity Profiles as a Function of κ_s^+
(Cebeci & Chang's Model)

in the log-law. The difference between van Driest's model with a changing parameter of B and Cebeci & Chang's model is recognized only in the region $y^+ < 20$ in the calculated velocity profiles. The velocity profiles calculated from Cebeci & Chang's model lie below those calculated from van Driest's model in this region of $y^+ < 20$. However, Cebeci & Chang's model cannot describe the velocity profile with a large constant A above the usual value of 5.29. Because all the experiments in this study were conducted over smooth and incompletely rough beds, i.e. $k_s^+ < 70$, it is considered that van Driest's model with a changing parameter of B can describe the velocity profile more adequately.

Using the velocity gradient dU/dy evaluated from the measured velocity distributions, the mixing length l was calculated from Eq. (5) and (6). An example of these results is shown in Fig. 9. The model curves of the mixing length calculated from Eq. (11) using the best-fitted value of B surely coincide with the experimental values. Therefore, it is concluded that the velocity distributions in steep open-channel flows can be well described by van Driest's mixing-length model, in which the damping coefficient B decreases in the supercritical flows.

Friction Coefficient f is defined as follows:

$$f = \frac{8ghI}{U_m^2} = \frac{8U_*^2}{U_m^2} \tag{16}$$

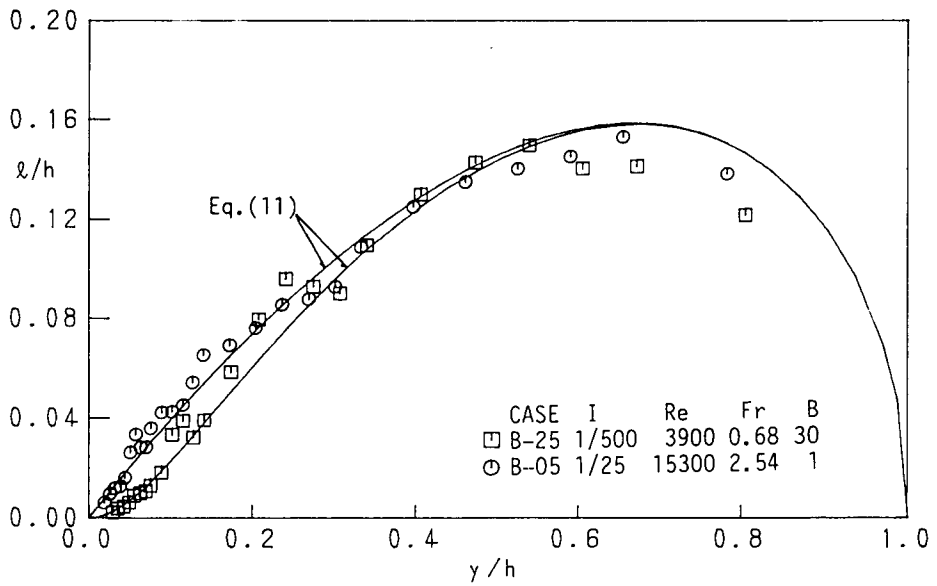

Fig 9. Distribution of Mixing Length in subcritical and supercritical flows

Fig. 10 (a) and (b) show the distributions of the friction coefficient f for smooth and rough beds, respectively. In these figures, the theoretical distribution for laminar flow:

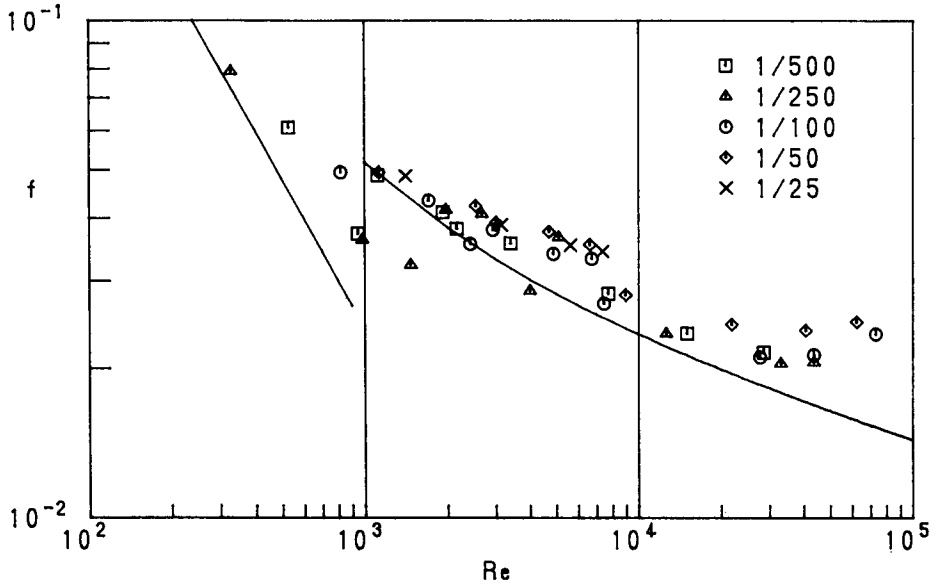

(a) smooth (cases A and C)

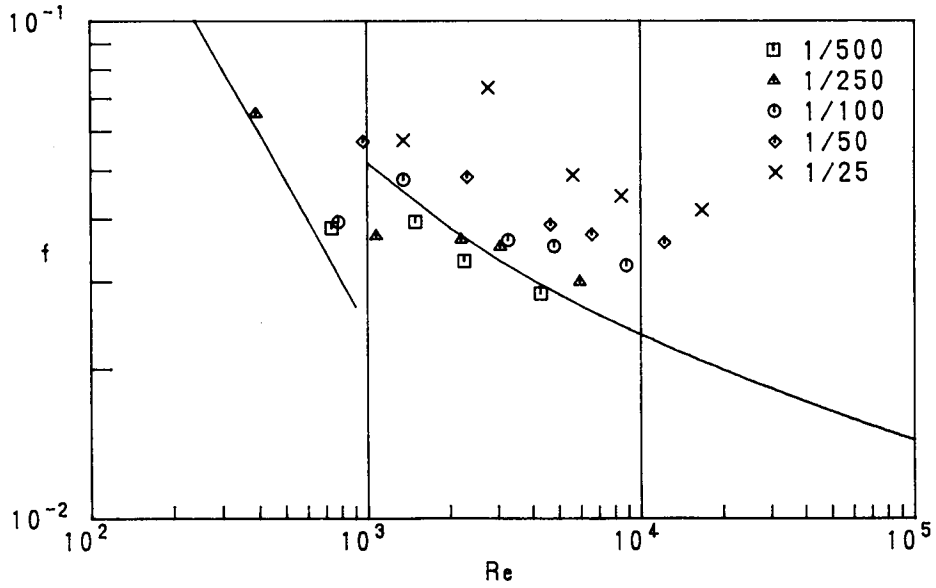

(b) rough (case B)

Fig. 10 Variation of frictin coefficient f aginst Reynolds Number

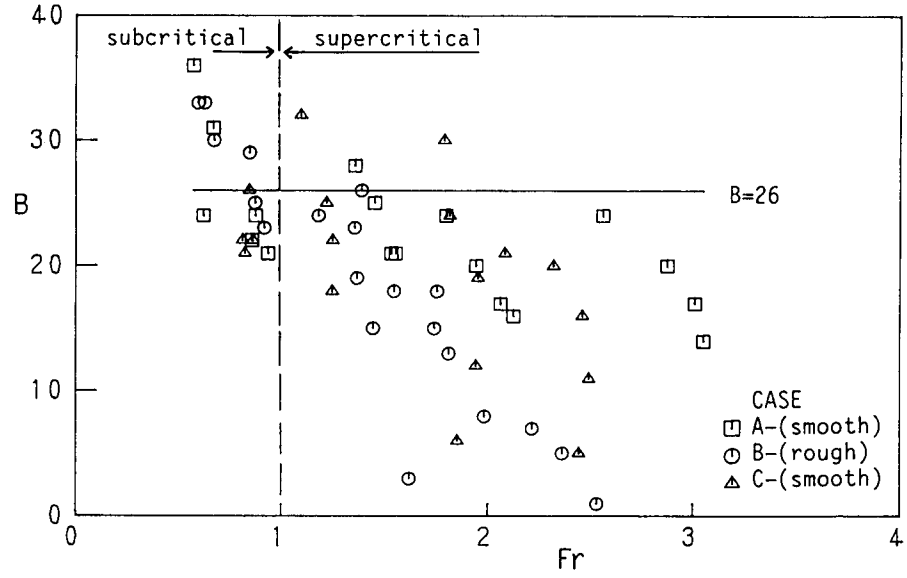

(a) against Froude Number

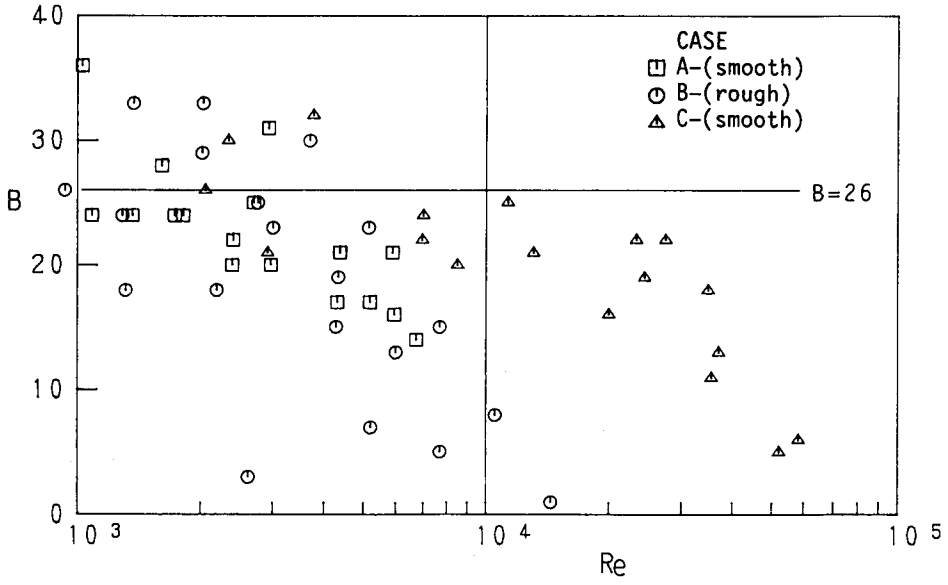

(b) against Reynolds Number

Fig. 11 Variation of Damping Coefficient *B*

$$f = 24/Re, \tag{17}$$

and that for a usual smooth trubulent flow calculated from Eq. (7), (10) and (11) with $B = 26$ are indicated. The values of f in the identical bed slope deviate from the curves for the usual smooth flow as the Reynolds number increases. The Reynolds number at which the experimental values deviate from the usual distribution becomes smaller as the bed slope increases and as the bed roughness increases. The increase of the friction velocity is, of course, a result of the velocity reduction, and explained by altering the damping coefficient B in van Driest's samping function.

Fig. 11 (a) shows the variation of the damping coefficient B against the Frude number Fr. The value of B decreases with an increase in the Froude number. This feature of B in Fig. 11 (a) is similar to that of A in Fig. 4, which implies the validity of Eq. (12). On the other hand, Fig. 11 (b) shows the relation between B and the Reynolds number Re. The value of B also tends to decrease with an increase of the Reynolds number in supercritical flows.

5. Decrease of Viscous-Sublayer Thickness in Steep Open-Channel Flows

Black (1969) examined the drag reduction phenomenon in turbulent flows of dilute polymer solutions. He suggested that the polymer additives increased the sublayer stability. Consequently, such a stability enlarged the thickness of the viscous sublayer, and then resulted in the increase of the mean velocity. The present phenomenon may be the opposite of the drag reduction. That is to say, in steep open-channel flows, the enlargement of the velocity scale in the wall region causes instability of the viscous sublayer, and consequently it apparently decreases the viscous-sublayer thickness.

It is important to find the proper parameters which control the variation of B in steep open-channel flows. As a result of multiple regression anaysis, the friction velocity U_* was proved to be a more predominant parameter than the Froude number. This fact seems to be reasonable because the behaviours of the viscous sublayer should be described by the inner parameters, i.e. the velocity scale U_* and the length scale ν/U_*. Fig. 12 shows the variation of B against U_* for a smooth bed and a rough bed. The value of B decreases with an increase of U_*.

The distribution of B versus U_* for rough beds is slightly different from that for smooth beds. This difference becomes larger with an increase of U_*. Any effect of the roughness should be involved in the behaviour of the damping coefficient B. The increase of the roughness size causes a decrease of the viscous-sublayer thickness, as has been graphically shown by Rotta (1950). The dimensionlessed

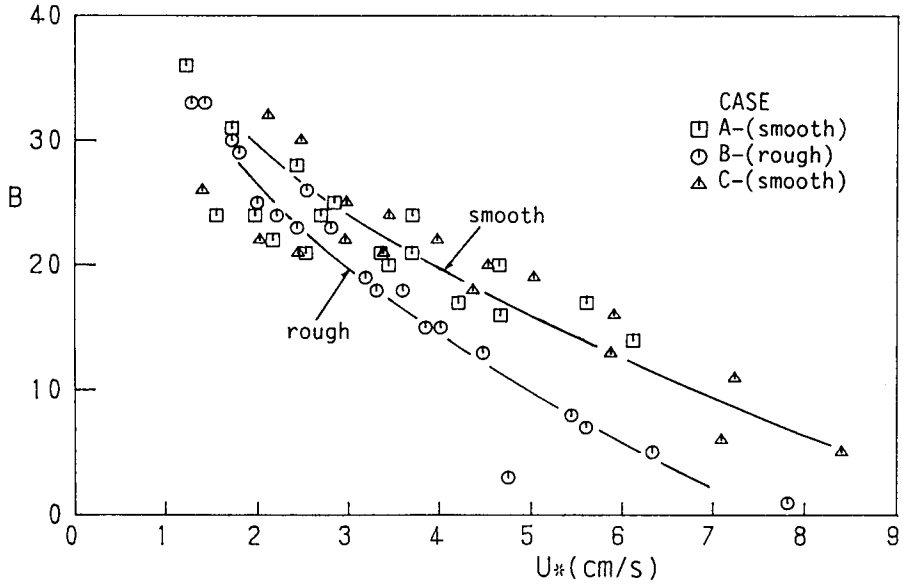

Fig. 12 Damping Coefficient B against Friction Velocity U_*

roughness size $k_s^+ \equiv k_s U_*/\nu$ becomes larger as the friction velocity U_* increases extremely. This equivalent sand roughness k_s was estimated here so that the integral constant A_r in the following log-law distribution for the rough bed might coincide with Nikuradse's experimental data.

$$U^+ = \frac{1}{\kappa} ln \frac{y}{k_s} + A_r \tag{18}$$

As a result, the averaged value of k_s was estimated as 0.4mm for sandpaper bed. Fig. 13 shows the variation of B against the roughness k_s^+. Although there is some scatter among the data of $k_s^+ < 10$, the values of B are approximately described by

$$B = 32\exp\{-(0.052k_s^+)^2\}, \qquad \text{for} \quad k_s^+ \leqq 35 \tag{19}$$

Fig. 13 also shows the calculated curve of Eq. (19). It should be emphasized here that van Driest's model with the damping coefficient B is limited up to the transition regime of roughness because the viscous sublayer disappears and the mechanism of turbulence production should be changed in the completely rough regime, as pointed out by Nakagawa & Nezu (1977).

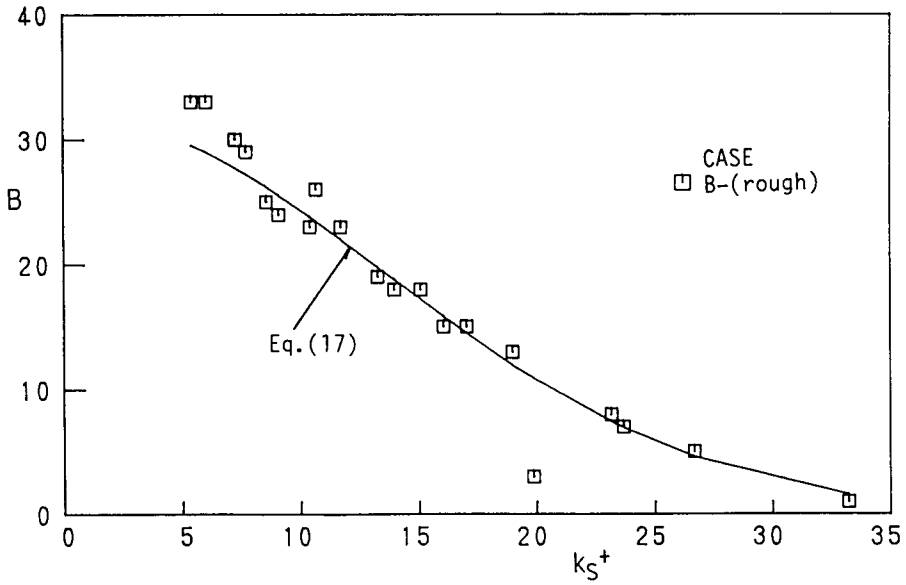

Fig. 13 Damping Coefficient B against Roughness Parameter k_s^+

6. Characteristics of Turbulence Intensity

Figs 14 (a), (b) and (c) show the distributions of u'/U_* against y^+ in the wall region ($y^+ \leqq 100$), as a function of the Froude number, over smooth and rough beds, respectively. The solid curves in these figures indicate the semi-empirical formula of u'/U_* proposed by Nezu (1977), which is described by

$$u'/U_* = D_u \exp(-\lambda_u \xi) \cdot \Gamma' + 0.3 y^+ \cdot (1 - \Gamma') \tag{20}$$

$$\Gamma' = 1 - \exp(-y^+/B'); \quad D_u = 2.26, \ \lambda_u = 0.88, \ B' = 10.$$

Γ' is the damping function for turbulence intensity similar to Γ in Eq. (10) for mean velocity. Nezu (1977) found that the damping coefficient B' for turbulence intensity should be chosen as $B' = 10$.

In the case of subcritical flow, the experimental values of u'/U_* coincide well with Eq. (20), as seen in Figs. 14 (a) and (b). On the other hand, in the case of supercritical flow, the experimental values of u'/U_* decrease with an increase of the Froude number. This decrease is especially predominant in the buffer region in which turbulence intensity attains a peak. Fig. 14 (c) indicates that the experimental values of u'/U_* decrease with an increase of the Reynolds number at a high Froude number ($Fr > 2$).

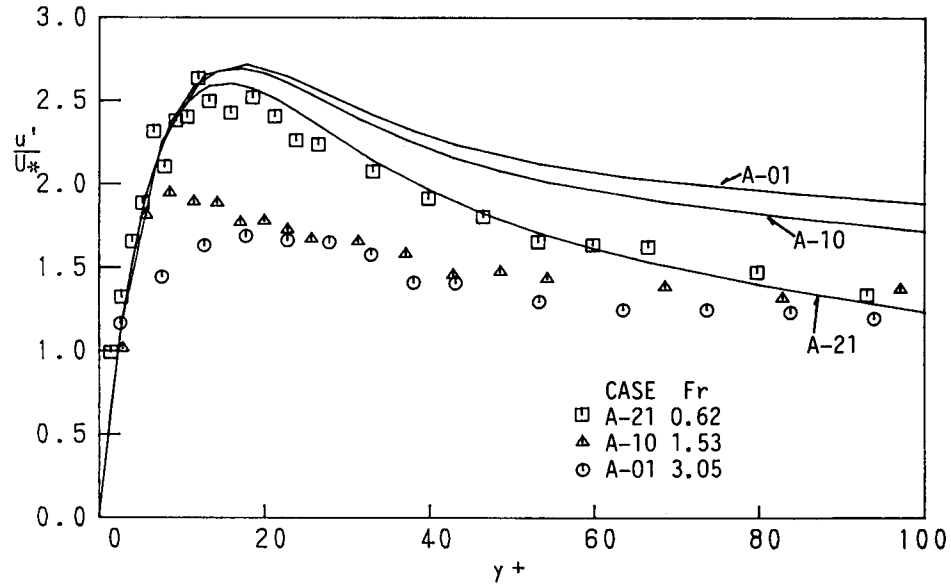

(a) Case A (smooth, flume A)

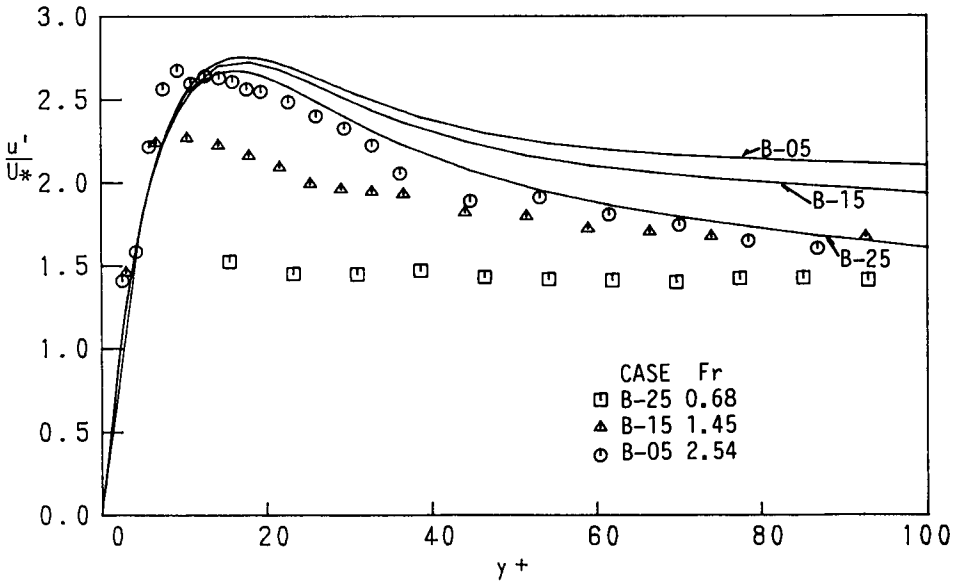

(b) Case B (rough, flume A)

Fig. 14 Distribution of Turbulence Intensity u'/U_* (inner variable description)

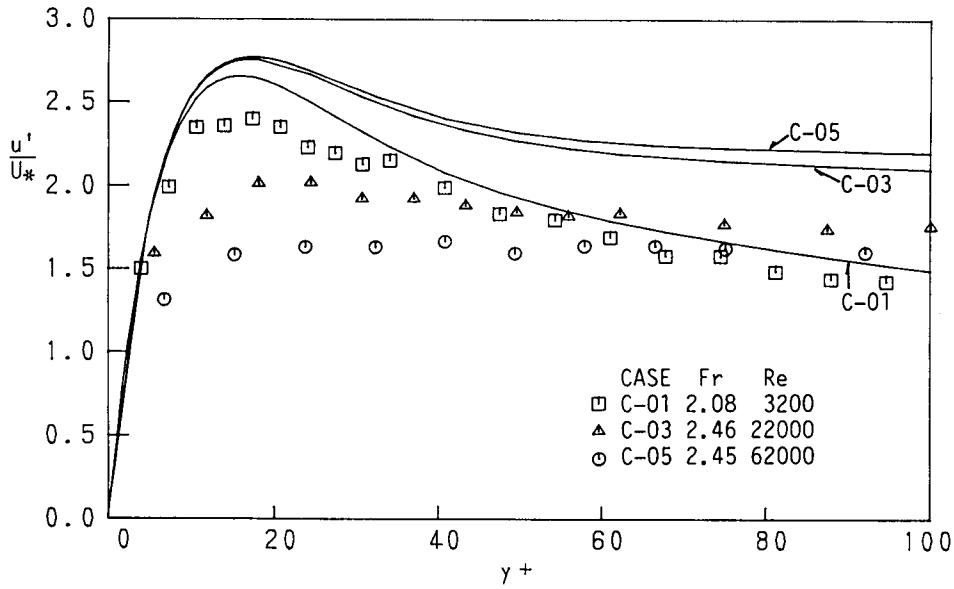

Fig. 14 (c) Case C (smooth, flume B)

Fig. 15 shows the distributions of u'/U_* against y/h in the case of **C**. The decrease of u'/U_* from the Eq. (20) occurs in the region $y/h < 0.3$, whereas the values of u'/U_* at $y/h > 0.3$ approximately coincide with Eq. (20). Consequently, the universal distribution of u'/U_* is no longer established in the near-wall region of the supercritical flows. On the other hand, the universal distribution is still valid in the region farther from the wall, i.e. $y/h > 0.3$.

It should be noted that the position at which u'/U_* deviates from Eq. (20) moves toward the wall with an increase of the Froude number. This feature is analogous with the reduction of the mean velocity profile shown in Fig. 2, and it seems to be related to the decrease of the viscous-sublayer thickness. The peak values u'_p of turbulence intensity is plotted against the variation of U_* in Fig. 16. The value of u'_p/U_* decreases with the increase of U_* in the same manner as the damping coefficient B.

The decrease of the viscous-sublayer thickness might affect the production mechanism of wall turbulence in the following aspect. The behaviour of the production of the turbulent evergy $G = -\overline{uv}(dU^+/dy^+)$ can be calculated using Eqs. (6), (7) and (10). Fig. 17 shows the calculated curves of G for $B = 26$ as a usual case and for $B = 10$ as a velocity-reduced case. The peak position of the energy

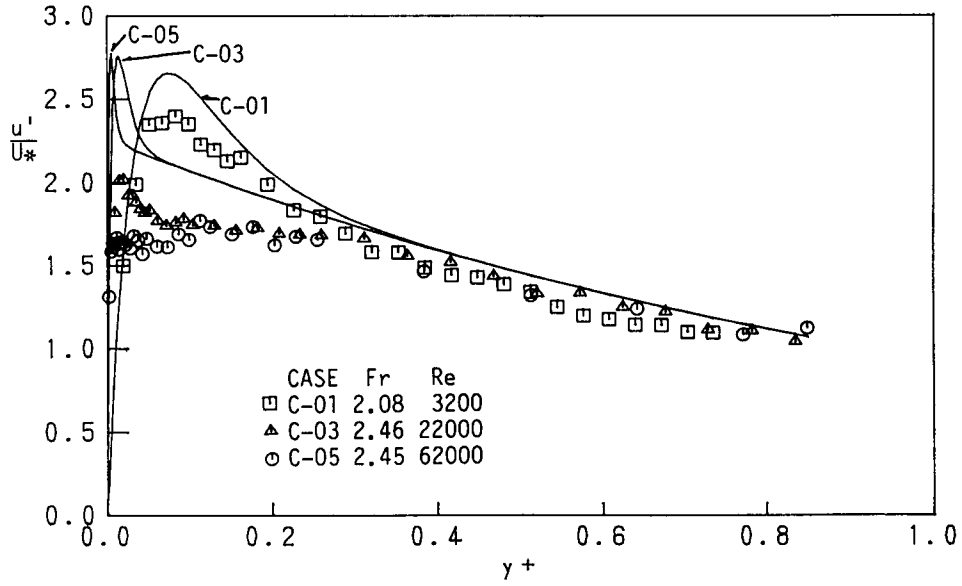

Fig. 15 Distribution of Turbulence Intensity u'/U_* (outer variable description)

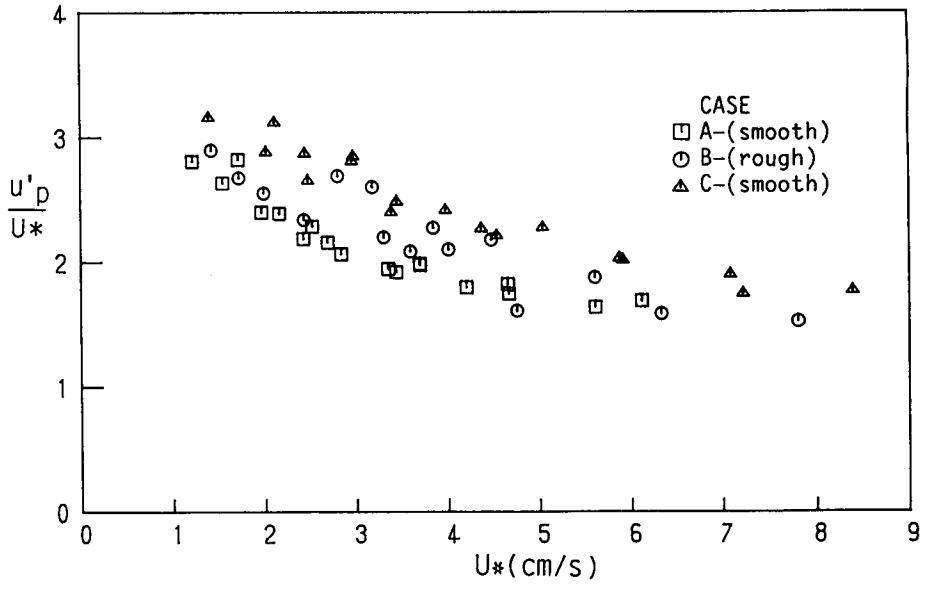

Fig. 16 Peak Value of Turbulence Intensity u'_p against Frition Velocity U_*

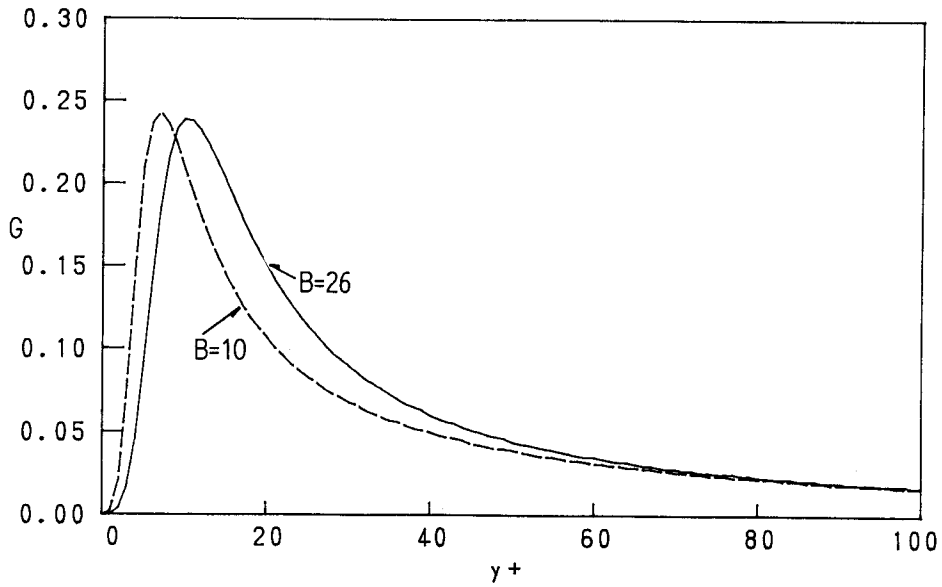

Fig. 17 Distribution of Productin Term G with the variation of B

production moves toward the bed, but the peak value itself chages little. Consequently, the value of the energy production decreases in the buffer region of $10 < y^+ < 40$. This fact is considered to be one reason why the decrease of turbulence intensity occurs near the bed in supercritical flows. More detailed examination of turbulence intensity is necessary to further verify these phenomena in supercritical flows.

Conclusions

Velocity measurements with a fiber-optic laser-Doppler anemometer were conducted in steep open-channel flows over smooth and incompletely rough beds. The results obtained in this study are summarized as follows:

(1) In steep open-channel flows, the integral constant A of the log-law distributions becomes smaller as the bed-slope becomes larger, while the von Karman constant κ is almost constant, i.e. $\kappa = 0.41$.

(2) From the velocity profiles very near the bed, it is suggested that the thickness of the viscous sublayer decreases in steep open-channel flows.

(3) Velocity profiles are well described by the mixing-length model using van Driest's damping function. In steep open-channel flows, the mixing length

becomes larger vary near the wall. This phenomenon can be expressed by adjusting the damping coefficient B in van Driest's damping function.

(4) The decrease of the damping coefficient B is governed by the increase of the friction velocity as well as the Froude number in supercritical flows. The variation of B is also expressed well by the dimensionless roughness size k_s^+.

(5) Turbulence intensity normalized by friction velocity decreases from the usual universal function near the bed in supercritical flows. The peak value of u'/U_* is correlated to the friction velocity U_*.

APPENDIX I. REFERENCES

Ashida, K., Daido, A., Takahashi, T. and Mizuyama, T. (1973): Study on the Resistance Law and the Initiation of Motion of Bed Materials in a Steep Slope Channel, Annual Bulletin of Disa. Prev. Res. Inst, Kyoto University, vol. 16-B, pp. 1–14 (in Japanese).

Black, T. J. (1969): Viscous Drag Reduction, Plenum Press, New York, pp. 383–407.

Cardoso, A. H., Graf, W. H. and Gust, G. (1989): Uniform Flow in a Smooth Open Channel, J. hydraulic Research, vol. 27, pp. 603–615.

Cebeci, T. and Chang, K. C. (1978): Calculation of Incompressible Rough-Wall Boundary Layer Flows, J. AIAA, vol. 16, pp. 730–735.

Coleman, N. L. and Alonso, C. V. (1981): Two-Dimensional Channel Flows over Rough Surfaces, J. Hydraulic Eng., ASCE, vol. 109, pp. 175–188.

Ishihara, T., Iwagaki, Y. and Goda, T. (1951): Studies on the Thin Sheet Flow, Proc. of JSCE, vol. 8, pp. 31–38 (in Japanese).

Iwagaki, Y. (1953): On the Laws of Resistance to Turbulent Flow in Open Smooth Channels, Proc of JSCE, vol. 16, pp. 22–28 (in Japanese).

Kanda, T. and Kikuri, M. (1979): Experimental Study on Resistance Law of Sheet Flows over Rough Surfaces, Proc. of 23rd Japanese Conference on Hydraulics, JSCE, pp. 339–346 (in Japanese).

Kanda, T. and Doi, K. (1981): Resistance to Shallow Flows in Rough Open Channels, Proc. of 25th Japanese Conference on Hydraulics, JSCE, pp. 105–112 (in Japanese).

Kirkgöz, M. S. (1989): Turbulent Velocity Profilers for Smooth and Rough Open Channel Flow, J. Hydraulic Eng., ASCE, vol. 115, No. 11, pp. 1543–1561.

Nakagawa, H. and Nezu, I. (1977): Prediction of the Contributions to the Reynolds Stress from Bursting Events in Open-Channel Flows, J. Fluid Mech., vol. 80, pp. 99–128.

Nezu, I. (1977): Turbulent Structure in Open-Channel Flows, Ph. D. Thesis, Kyoto University.

Nezu, I. and Rodi, W. (1985): Experimental Study on Secondary Currents in Open Channel Flow, Proc. of 21st Congress of IAHR, Melbourne, vol. 2, pp. 19–23.

Nezu, I. and Rodi, W. (1986): Open Channel Flow Measurements with a Laser Doppler Anemometer, J. Hydraulic Eng., ASCE, vol. 112, pp. 335–355.

Nezu, I., Nakagawa, H. and Rodi, W. (1989): Significant Difference of Secondary Currents in Closed Channels and Narrow Open Channels, Proc of 23rd Congress of IAHR, Ottawa, pp. A125-A132.

Rotta, J. C. (1972): Turbulente strömungen, B. G. Teubner, Stuttgart.

Rotta, J. C. (1950): Das in Wandnähe gültige Geschwindigkeitsgesetz turbulenter Strömungen, Ing. Arch., vol. 18, pp. 277–280.

Schlichting, H. (1979): Boundary-Layer Theory, McGraw-Hill.

Sill, B. L. (1982): New Flat Plate Turbulent Velocity Profile, J. Hydraulic Eng., ASCE, vol. 108, pp. 119–130.

Tominaga, A., Nezu, I., Ezaki, K. and Nakagawa, H. (1989): Three-Dimensional Turbulent Structure in Straight Open Channel Flows, J. Hydraulic Research, vol. 27, No. 1, pp. 149–173.

Tominaga, A. and Nezu, I. (1991): Turbulent Structure in Compound Open Channel Flows, J.

Hydraulic Eng., ASCE vol. 117, pp. 21–41.
Vedula, S. and Achanta, R. R. (1985): Bed Shear from Velocity Profiles: a New Approach, J. Hydraulic Eng., ASCE, vol. 111, pp. 131–143.
Wills, J. C. (1985): Near-Bed Velocity Distribution, J. Hydraulic Eng., ASCE, vol. 111, pp. 741–753.

APPENDIX II. NOTATION

The following symbols are used in this paper:

A = integral constant in the log-law
B = damping coefficient in van Driest's damping function
B' = damping coefficient in semi-empirical function of u'/U_*
b = channel width
Fr = Froude number ($= U_m/\sqrt{gh}$)
g = gravitational acceleration
h = flow depth
I = bed slope
ks = equivalent sand roughness
ks^+ = $U_* ks/\nu$
l = mixing length
Re = Reynolds number ($= U_m h/\nu$)
U = mean velocity
U_m = mean bulk velocity
U_* = friction velocity
U^+ = U/U_*
U' = turbulence intensity in streamwise direction
y = vertical coordinate from the bed
y^+ = $U_* y/\nu$
Γ, Γ' = damping function
κ = von Kármán constant
ρ = density of water
ν = kinetic viscosity
ξ = y/h